Monte Carlo simulation of three-dimensional islands

Sovirith Tan and Pui-Man Lam
Department of Physics, Southern University, Baton Rouge, Louisiana 70813
(Received 16 November 1998; revised manuscript received 12 February 1999)

The usual kinetic Monte Carlo method is adapted, to treat off-lattice problems of multilayer growth (coverage $\theta>1$) by molecular-beam epitaxy. This method takes into account the Schwoebel barrier, which comes out as a result of the choice of the potential interaction between the atoms. This method allows a free choice of the lattice mismatch, temperature, deposition flux rate, and interfacial energies. A particular choice of these parameters leads to the three-dimensional (3D) (Volmer-Weber) growth mode, whereas another choice of these parameters leads to the 2D-3D growth mode (Stranski-Krastanov). The 3D islands seem to obey scaling only approximately. Using this method, the surface stress inside a substrate and a (pyramidal) coherent 3D island is computed. Strong relaxations appear, not only at the edges of the 3D island (which is expected), but also in the proximity of the edges, and inside the 3D island. These particular sites inside the 3D island are located just beneath a step site of the upper layer. Moreover, these particular sites develop strong corrugations, which later are propagating along the layer. Strain-induced modulation of layers is thermally activated, so the steps could act as defects and nucleation sites for propagating roughness, in agreement with some theories and experimental facts. [S0163-1829(99)16731-6]

I. INTRODUCTION

The realization of electronic and magnetic devices requires a sophisticated technology, able to grow perfect layers at the interface. It is known that the use of lattice-mismatch materials (variable semiconductor band gap, carrier mobility etc.) offers a wider range of technological applications. But the growth of lattice-mismatch semiconductor systems often proceeds via the two-dimensional–three-dimensional (2D-3D) Stranski-Krastanov mode,[1] where the growth of a few coherent wetting layers is interrupted by the nucleation of 3D islands on top of the wetting layers. On the other hand, the discovery of coherent, dislocation-free 3D islands,[2] with a very uniform size distribution, has drawn much attention to this 2D-3D growth mode as a method to provide self-assembled quantum dots[3] (for the manufacture of quantum dots laser, for example). Finally, if the lattice mismatch is very large and the interfacial energy high enough, the 3D islands can grow directly on top of the substrate: it is the 3D (Volmer-Weber) growth mode.[4]

In Ref. 5, the mean-field rate equations are used to find the growth dynamics and maximum island density. Their models take into account deposition flux, adatom diffusion, aggregation and sticking probability to the island, and desorption. In Ref. 6, the authors investigated the formation of 3D islands, including evaporation and trapping near surface defects. To this aim, they combined a scaling analysis, rate equations, and a Monte Carlo computer simulation. The computer simulation allows them to predict the island size distribution. In Ref. 7, the authors carried out self-consistent rate equations to investigate the formation of coherent 3D islands during semiconductor heteroepitaxy. Their model uses the 2D island critical size i^* as an atomistic parameter. The 3D island density dependence on coverage and growth rate are computed.

In a usual kinetic Monte Carlo simulation of a solid-on-solid model, the Schwoebel barrier[8] has to be put by hand as a variable parameter appearing in the hopping rate of an Arrhenius form, as for example in Ref. 9, where the authors successfully simulated the reentrant layer-by-layer growth of Pt/Pt(111). Also, in the usual kinetic Monte Carlo simulations, the effect of lattice misfit on the distribution of islands size, in Ref. 10 for example, enters only through an additional barrier for detachment of adatoms from the islands. In this paper, where a method is developed to treat off-lattice problems, the Schwoebel barrier comes out as a result of the choice of the interaction potential between the atoms of the upper and lower layers. In this model, each atom tries a virtual move around its immediate neighborhood, before an effective move is performed. The future move of each atom depends on its very environment. The Schwoebel barrier is then ''felt'' by each atom because any move in the direction of a descending step is energically unfavorable, and so is hindered. Moreover, using this method, the effect of the lattice mismatch results simply from the very choice of the size of the adatom σ_{aa} and the substrate σ_{ss} appearing in the interaction potential [cf. Eq. (1)]. By changing relevant parameters like the lattice-misfit size, temperature, flux, and interfacial energy, the interaction between the atoms and also the environment felt by the atoms are changed. This changes the Schwoebel barrier and also the growth mode.

II. METHODS

The usual kinetic Monte Carlo method is adapted, to avoid the restriction of the solid-on-solid model, and to tackle off-lattice problems. Each atom, deposited at constant flux F, temperature T, and diffusion constant D, is moving freely on a square lattice. This model enables us to simulate deposition, diffusion, aggregation, detachment from islands, desorption, and island growth and coalescence at low and high coverages ($\theta<1$ and $\theta>1$). This model[11] takes also into account the Schwoebel effect, when adatoms are deposited on top of islands.

In this model, the square lattice substrate is kept fixed. Each adatom-adatom (a-a) pair and each adatom-substrate atom (a-s) pair interact through a generalized Lennard-Jones (m,n) potential:[12]

$$\Phi(q)=E\frac{q^n-nq}{n-1},\quad q=\left(\frac{\sigma}{r}\right)^m, \tag{1}$$

where E is the energy parameter, σ the size of the atom, and r the interatomic distance. We have fixed $m=2$ and $n=1.4$ for the adatom-adatom (a-a) pair, and $m=2$ and $n=1.25$ for the adatom-substrate atom (a-s) pair. This model was used for the simulation of lead on copper: Pb/Cu(100).[12]

At each Monte Carlo step, the probability P_d for adding a new particle to an assembly of N particles, is computed:

$$P_d=\frac{F}{F+\Sigma_{i=1}^{N}D(T)\exp(-E_i/kT)},$$

with

$$D(T)=\left(\frac{2kT}{h}\right)\exp\left(-\frac{E_s}{kT}\right)\Big/A, \tag{2}$$

where F is the flux; E_i the bond energy of atom i, due to its in-plane neighbors, and T the temperature. $D(T)$ is the adatom diffusion rate divided by the total number A of lattice sites on the surface, k is the Boltzmann's constant, and h is the Plank's constant. The energy E_s is determined from the usual minimal energy path saddle-point method:[13] a test atom is moved to a neighboring binding site in small steps, and the adatom energies are recorded at each step. The sum of E_i and E_s results in the energy difference between the saddle-point configuration and the minimum (equilibrium) configuration. So this sum is the diffusion activation energy, as expected. In other words, the sum of E_i and E_s is the energy barrier for every possible atomic configuration that an adatom can encounter. The energy E_i and E_s must be computed for each atomic configuration. The computation of E_s is made easier by the fact that the adatom, left alone on the square lattice, occupies mainly two sites, the ''hollow'' site and the ''bridge'' site. In the case of lattice misfit between the adsorbate and substrate, these two sites are slightly shifted, so the energy E_s is corrected consequently. This method enables sites of potential minima to be established. For example, for the 0% lattice-mismatched case, the result $E_s=1.4$ eV was obtained. If the temperature is fixed at $T=800$ K, and the flux fixed at $F=0.13$, a value $D/F=5\times10^5$ is obtained.

The hopping probability P_h is therefore

$$P_h=1-P_d=\frac{\sum_{i=1}^{N}D(T)\exp(-E_i/kT)}{F+\sum_{i=1}^{N}D(T)\exp(-E_i/kT)}. \tag{3}$$

If the deposition of a new particle is not allowed, then an adatom i, chosen at random among the N adatoms already deposited, is allowed to diffuse. Precisely, this adatom i is allowed to perform a virtual random move within a cube, of size smaller than 1/10 of the interatomic distance, centered at this adatom i. Then the atomic interaction energies, before and after moving, are compared, and the final position is accepted or rejected according to the Boltzmann probability $p=\exp(\Delta E_i/kT)$ where ΔE_i is the energy difference for atom i in the both considered successive configurations. If the move of atom i is accepted, then we go ahead and a new deposition probability P_d is computed. If the move of atom i is rejected, another adatom is tried, until a move is performed with success. Then we go on and compute a new deposition probability P_d. The coverage $\theta=Ft$ gives a measure of the physical time.

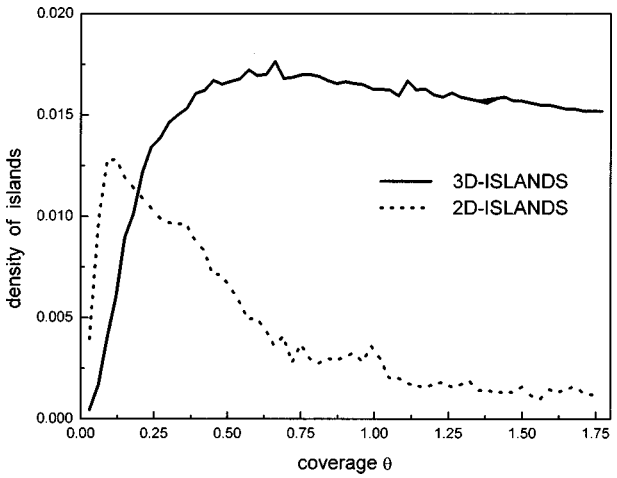

FIG. 1. Density of 2D and 3D islands for a 3D (Volmer-Weber) growth mode and a lattice misfit of 10%, at temperature $T=600$ K and flux rate $F=0.1$.

III. 3D (VOLMER-WEBER) GROWTH MODE

Which growth mode will be adopted in a given system may be guessed roughly on the basis of interfacial free-energy considerations (sometimes, such a guess is not easy: see, for example, Ref. 14). For example, a high interfacial energy is likely to drive the system to a 3D (Volmer-Weber) growth mode: the epilayer will not wet the substrate. So, to simulate a 3D growth mode, suitable interface energy, lattice misfit, temperature, and flux rate parameters are chosen:

$$E_{aa}=1.25E_{as},\quad \sigma_{aa}=0.9\sigma_{ss}\quad \text{(a misfit at 10\%)},$$
$$T=600\ \text{K},\quad F=0.1,$$

where E_{aa} (E_{as}) is the energy parameter between an adatom and an adatom (substrate atom), σ_{aa} (σ_{ss}) is the size of an adatom (substrate atom), T is the temperature, and F is the flux rate. A square lattice size 150×150 is fixed.

Figure 1 shows the dependence of the island distribution on the coverage, for a 3D growth mode. The density of 2D islands increases quickly up to coverage $\theta=0.1$, and falls off. At the same time, the density of 3D islands rises sharply, and reaches roughly a saturation value at coverage $\theta=0.4$. Experimentally, a very steep increase of the 3D island density was observed in the case of coherent 3D islands,[15] and this steep rise was also computed from self-consistent rate equation.[7] Beyond a coverage $\theta=1$, a slight decrease of the 3D island density is seen in Fig. 1, and is attributed to the coalescence of some smaller 3D islands.

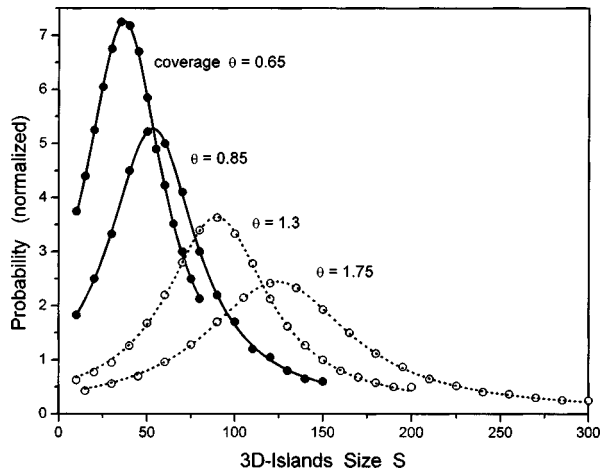

FIG. 2. Distribution of 3D island size for a 3D (Volmer-Weber) growth mode and a lattice misfit of 10%, at temperature $T=600$ K and flux rate $F=0.1$.

Figure 2 exhibits the size distribution of 3D islands. At a submonolayer coverage ($\theta<1$), the 3D island size distribution is rather narrow. At a higher coverage ($\theta>1$), the size distribution broadens. This size distribution broadening is explained by the fact that, at higher coverage, the 3D islands are larger and more liable to generate defects and dislocations. Large islands, with defects and dislocations, grow and expand more freely, which results in a polydispersity of size.

Finally, Fig. 3 represents the scaled distribution $N(S)\langle S\rangle^2/\theta$, for coverage $\theta=0.85$, $\theta=1.3$, and $\theta=1.75$, where S is the size of the 3D island, and $N(S)$ is the number of 3D islands of size S. The three curves, for the different coverages, seem to fall approximatively onto a single scaling function, although the peak experiences a 50% increase. The scaling assumption, largely valid for 2D islands,[17] seems here to hold only approximately for 3D islands. Meanwhile, Ref. 16 reported the validity of the scaling assumption for 3D island in InAs/GaAs.

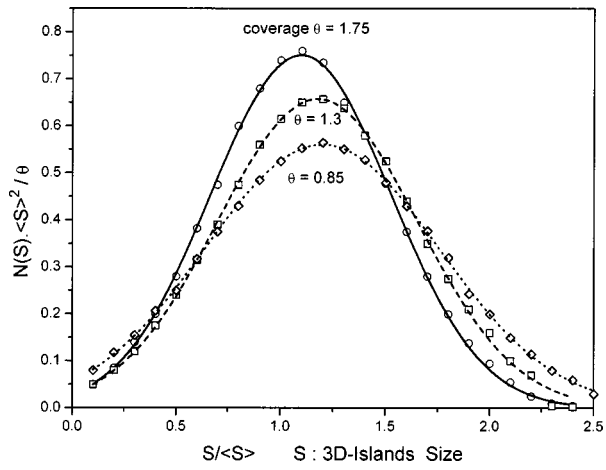

FIG. 3. Scaled distribution of 3D island size: $N(S)\langle S\rangle^2/\theta$, where S is the 3D island size, $\langle S\rangle$ is the average island size, and $N(S)$ is the number of 3D islands of size S, at different coverages $\theta=0.85$, 1.3, and 1.75, for a 3D (Volmer-Weber) growth mode and a lattice misfit of 10%, at temperature $T=600$ K and flux rate $F=0.1$.

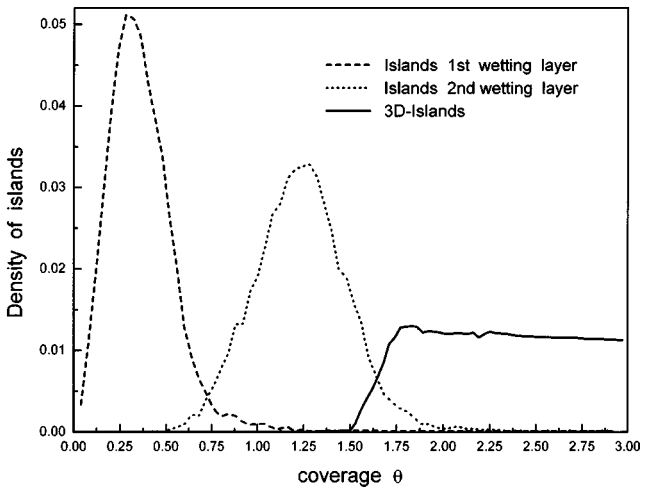

FIG. 4. Density of islands for a 2D-3D (Stranski-Krastanov) growth mode and a lattice misfit=0%, at temperature $T=700$ K and flux rate $F=0.1$. After the completion of two complete wetting layers, 3D islands appear at a coverage $\theta=1.5$.

IV. 2D-3D (STRANSKI-KRASTANOV) GROWTH MODE

To change the growth mode, the relevant parameters (like lattice misfit, interfacial energy and deposition temperature) have to be changed. The particular case of homoepitaxy (the lattice misfit is 0%) has been selected. A square 100×100 lattice was chosen. The following parameters were fixed:

$$E_{aa}=E_{as},\quad \sigma_{aa}=\sigma_{ss}\quad (\text{misfit}=0\%),$$

$$T=700\ \text{K},\quad F=0.1.$$

In a particular case of homoepitaxy (the misfit is 0%), a 2D growth mode (Frank–van der Merwe[18]) would reasonably be expected. In fact, we have obtained a 2D-3D (Stranski-Krastanov) growth mode; the growth was two dimensional only for the first two layers, and 3D islands appear at coverage $\theta=1.5$. This unusual result is attributed to the strong Schwoebel barriers, which were already reported[11] for the present model. A simulation, at a higher temperature $T=800$ K, gives the same 2D-3D growth mode. In particular, the second wetting layer is seen to be in a degraded state, more liable to generate defects and dislocations, paving the way for the formation of 3D islands. Experimentally, the 2D-3D growth mode has been witnessed in homoepitaxial systems, like Pt/Pt(111).[19]

Figure 4 displays the density of islands for the first two wetting layers, and the density of 3D islands at a later stage (2D-3D growth mode). As expected, the first layer is complete at coverage $\theta=1$, and the second layer is complete at coverage $\theta=2$. The second layer starts to build up as early as $\theta=0.5$. The first layer reaches its maximum island density not at coverage $\theta=0.5$ but at coverage $\theta=0.3$. Finally, the 3D islands appear at coverage $\theta=1.5$, and reach their saturation density at coverage $\theta=1.75$. The 3D-island density experiences a slight decrease at subsequent stages, because

of the coalescence of some 3D islands. The sharp rise of the 3D-island density, at a threshold coverage, was reported experimentally.[15]

The evidence that the kinetic Monte Carlo method, described here, incorporates the Schwoebel barrier, is given by the damping of the simulated reflection high-energy electron-diffraction (RHEED) oscillation intensity. Because of the glancing geometry of RHEED,[20] only the first few layers of the material interact with the electrons. So RHEED is rather sensitive to the surface morphology (roughness, distribution of islands, steps, terraces, etc., on the surface). The RHEED oscillation is due to a cyclic transition from smooth to a rough surface, and vice versa, and so the RHEED oscillation is currently used to check the 2D growth mode. In Ref. 21, it was shown by the authors that the RHEED intensity depends inversely on the surface step density, and this fact was used to simulate the RHEED intensities by Monte Carlo methods.[21,22] In the present paper, the RHEED intensities are computed through the following formula, giving the diffracted intensity from a surface:

$$I(Q)=\left|\sum_{\text{atom } i \text{ in upper layer}} \exp(iQr_i)\right|^2, \qquad (4)$$

where $Q=k_f-k_i$ is the transferred wave vector, obtained by the Ewald construction. Only the waves scattered by the atoms of the upper layers, interacting with the RHEED electrons, are included in the summation. It is assumed here that the scatterers are all identical, and that multiple-scattering events are neglected. It is also assumed that the contribution of the positive step is the same as the contribution of the negative step, although this is not quite true.

Figure 5(a) shows the simulated RHEED intensities for the 2D-3D (Stranski-Krastanov) growth mode described previously. The oscillation amplitude is damped because the growth is not restricted to a single layer at a time, and the nucleation of a new layer can start before the preceding layer is complete, illustrating the Schwoebel effect incorporated in this model (in Fig. 4, the second layer starts at coverage $\theta=0.5$ and the 3D islands appear at $\theta=1.5$). Figure 5(b) displays the RHEED intensities for the 3D (Volmer-Weber) growth mode. The sharp decrease of the RHEED intensity at the beginning is due to the formation of the 3D islands. At further stages, the RHEED intensity does not show wide variations because, during the subsequent growth of the 3D islands, the roughness looks very much the same.

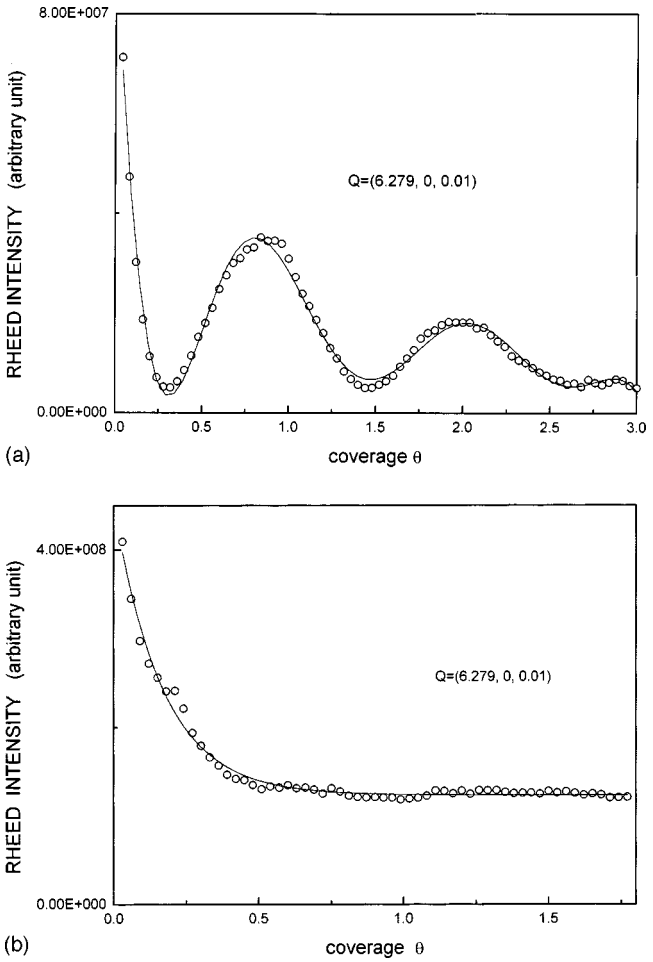

FIG. 5. (a) RHEED intensity for a 2D-3D (Stranski-Krastanov) growth mode and a lattice misfit of 0%, at temperature $T=700$ K and flux rate $F=0.1$. (b) RHEED intensity for a 3D (Volmer-Weber) growth mode and a lattice misfit of 10%, at temperature $T=600$ K and flux rate $F=0.1$.

V. COMPUTATION OF SURFACE STRESS INSIDE A COHERENT 3D ISLAND. CORRUGATION OF THE UPPER LAYERS

We chose to form a dislocation-free 3D island, of square base 80×80, of pyramidal shape and a height of $h=8$ ML. This coherent 3D island is laid on two wetting layers, of size 100×100, and exhibiting a low lattice misfit of 0.5% with the substrate. The profile can be seen in Fig. 6(a). Thus the present system consisting of two wetting layers plus the coherent 3D island (of height 8 ML) is relaxed by means of molecular-dynamics methods. The Verlet algorithm was used to implement the molecular-dynamics simulation. The periodic boundary condition was applied for a simulation cell of size 100×100. The temperature is kept constant at $T=700$ K, by rescaling the velocities of all the atoms. This method gives good results,[12] although a more correct way is to use the thermostat method of Nose and Hoover.[23] A total of 30 000 atoms are allowed to relax at fixed temperature.

The strain field, inside coherent 3D islands, was studied within the continuum elasticity theory, with the help of finite-element (FE) methods[24] or other methods.[25] Density functional theory[26] has been used to find the strain field inside coherent epilayers. In Ref. 27, the authors calculated in particular the strain at the island edges in order to investigate the transformation of 2D platelets to 3D islands. The FE methods give good results for an extended atomic plane and semi-infinite stripes. If the whole size decreases, singular sites, like wedges, apex, etc., may appear. At these singular sites, the FE methods may give ambiguous solutions, and the mesh grid has to be kept small enough, so more computations are required.

The authors of Ref. 28 use molecular-dynamics methods, to investigate the stress field inside the wetting layers and the undislocated 3D islands of the Ge/Si system. In the present paper, the same virial formula will be used to compute the stress tensor inside the two wetting layers and the coherent 3D island (of height 8 ML):

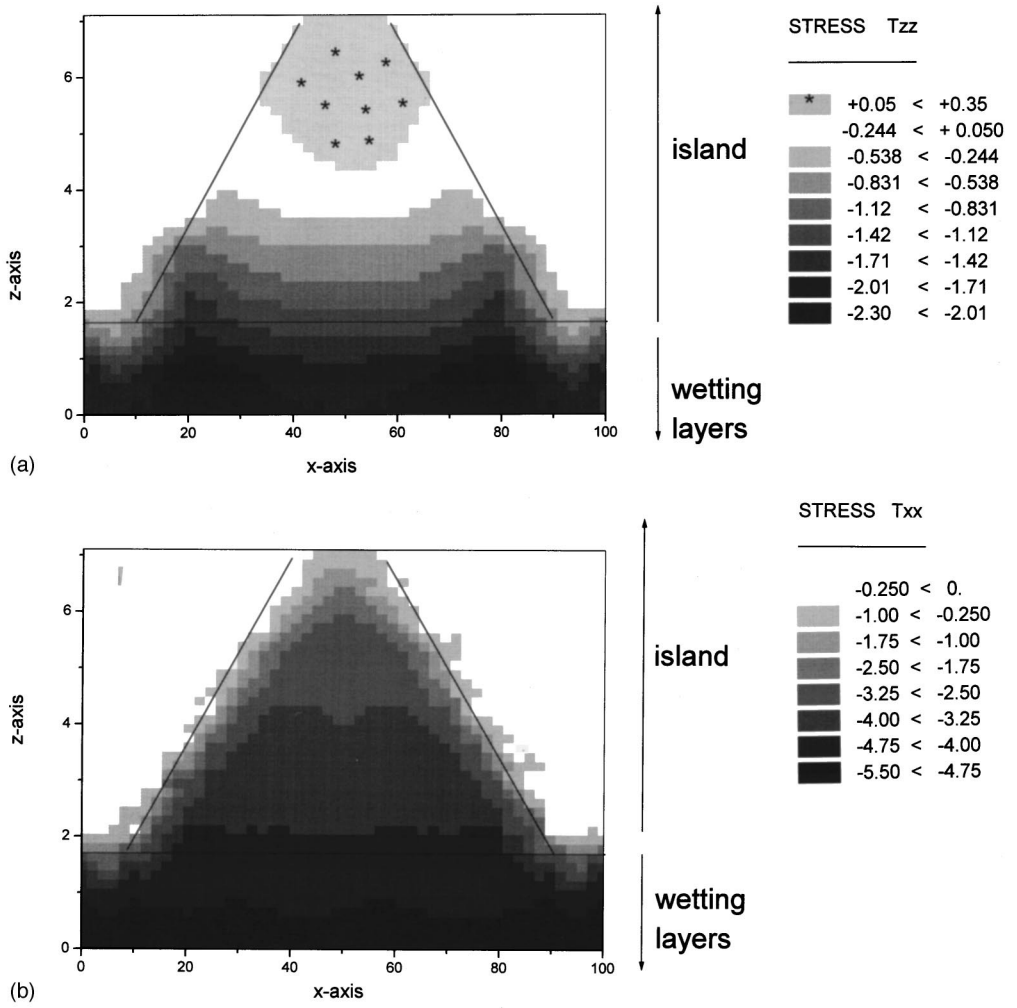

FIG. 6. (a) Distribution of the stress field T_{zz} inside the coherent 3D island (of height $h=8$ ML and a base of 80×80) and inside the two wetting layers (of size 100×100). The two wetting layers are lying on a 100×100 fixed substrate, located at $z=0$. The lattice misfit is 0.5%, and temperature $T=700$ K. The top, edges, and wedges of the 3D islands are strongly relaxed. (b) Distribution of the stress field T_{xx} inside the coherent 3D island (of height $h=8$ ML and a base of 80×80) and inside the two wetting layers (of size 100×100). The two wetting layers are lying on a 100×100 fixed substrate, located at $z=0$. The lattice misfit is 0.5%, and temperature $T=700$ K. The top, edges, and wedges of the 3D islands are strongly relaxed.

$$T_{\alpha,\beta}=\sum_{k=1,N}\left\{-mv_k^{\alpha}v_k^{\beta}+\tfrac{1}{2}\sum\sum_{j\neq k}r_{jk}^{\alpha}\,\mathrm{grad}^{\beta}\,\Phi(r_{jk})\right\}, \tag{5}$$

where $\alpha,\beta=x,y,z$, and v_k is the velocity of atom k and r_{jk} is the vector directed from atom j to atom k, and $\Phi(r_{jk})$ is the interaction between atom j and k.

Figure 6(a) [Fig. 6(b)] shows the stress field T_{zz} (T_{xx}) inside the wetting layers and the coherent 3D island. The stress, built up at the interface, inside the wetting layers, is progressively relieved through the 3D island. As can be seen in Figs. 6(a) and 6(b), the edges of the 3D island and the wedges (at the junction of the edges of the 3D island and of the wetting layers) experience a strong relaxation. Particularly at the wedge between the 3D island and the wetting layers, there is a steep stress gradient. As represented on Fig. 6(a), the top of the 3D island is slightly overrelaxed, and the stress turns a little tensile at the top. In Fig. 7(a) [Fig. 7(b)] is shown the stress T_{zz} (T_{xx}) inside each layer of the wetting layers and of the 3D island. It is easily noticed that, at the wedges, a significant relaxation is found. The stress is progressively relieved inside the 3D island, in conformity with the expected strain relaxation through the island. The behavior of the stress at the particular sites (like the wedge at the interface wetting-layer/3D island, or the top of the 3D island) is remarkable because the atomistic nature of the wetting layers and of the 3D islands cannot be dismissed at these sites. So it could be argued that molecular-dynamics methods may be helpful to investigate these particular sites, where the steep stress gradient and inhomogeneous concentrations of stress and strain make continuum theories approach difficult.

For example, in Fig. 7(b), the stress values T_{xx} at the edges of the 3D-island layers are relaxed to a common value $T_{xx}=0$, already predicted by continuum theories like FE.[24,25] Here what is new is the other relaxation inside the layer, just beneath the step site of the upper layer. In Fig. 7(b), the values of this inside relaxation take a parabolic shape, as the values are taken from the different layers of the 3D island.

We decide to have a closer look at these sites, which show a strong inside relaxation. Figure 8 represents two snapshots of the z profile of the 3D islands, of base size 60×60 and 4 ML high, laying on two wetting layers (of size 80×80), with

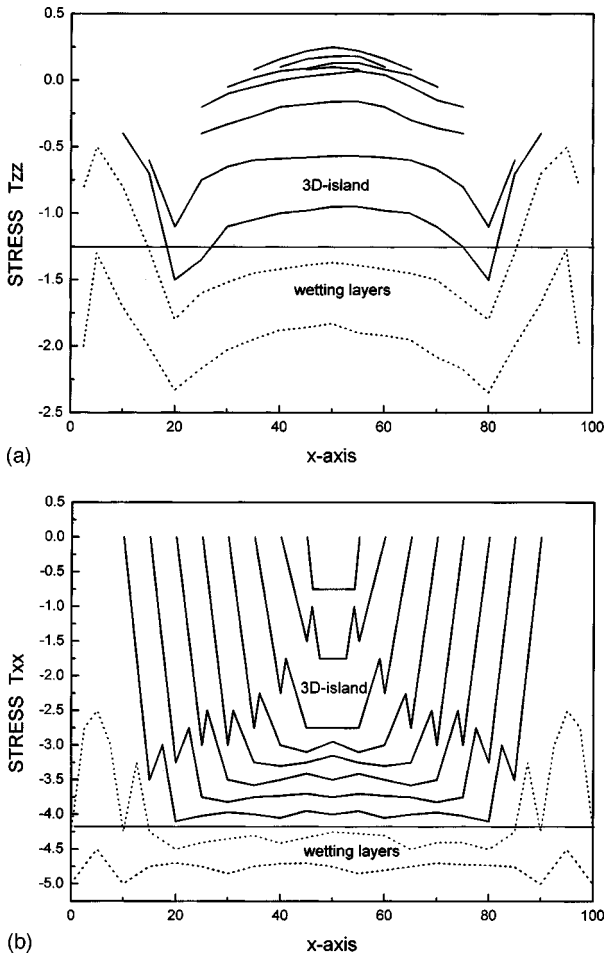

FIG. 7. (a) Stress field T_{zz} inside each layer of the coherent 3D island (of height $h=8$ ML and a base of 80×80) and of the two wetting layers (size 100×100). The two wetting layers lie on a 100×100 fixed substrate. The lattice misfit is 0.5%, and temperature $T=700$ K. The top, edges, and wedges of the 3D islands are strongly relaxed. Notice the inside relaxation of parabolic shape. (b) Stress field T_{xx} inside each layer of the coherent 3D island (of height $h=8$ ML and a base of 80×80) and of the two wetting layers (size 100×100). The two wetting layers lie on a 100×100 fixed substrate. The Lattice misfit is 0.5%, and temperature $T=700$ K. The top, edges, and wedges of the 3D islands are strongly relaxed. Notice the inside relaxation of parabolic shape.

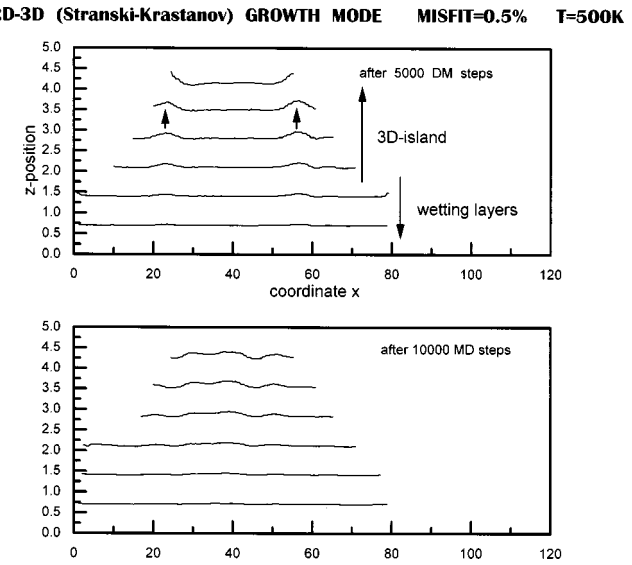

FIG. 8. Snapshots of the z profile of the coherent 3D island (a height of 4 ML, and a base of 60×60) and of the two wetting layers (size 80×80). The two wetting layers are lying on a fixed substrate located at $z=0$. The snapshots are taken after 5000 and 10 000 MD steps. The ''hilly'' bumps are built up near the edges of the 3D island, just beneath the step site of the upper layer. The bumps are attenuated near the wetting layers. The initial bump promotes further corrugations propagating along the layers.

a lattice mismatch of 0.5% and at a temperature $T=500$ K. These pictures are recorded after 5000 molecular-dynamics (MD) steps and 10 000 MD steps. After 5000 MD steps, some ''hilly'' bumps are built up at some particular sites of the 3D island, near the edges, just beneath the step site of the upper layer above, as indicated by arrows on Fig. 8. The sites showing a strong stress relaxation inside the layers are also those displaying strong corrugations. The bumps, strong at the top of the 3D island, are attenuated at the interface with the wetting layers. After 10 000 MD steps, the hilly bumps, previously located near the edge of the 3D island, are running along the upper layers of the 3D island, and the layer at the base of the island is only slightly affected.

The hypothesis of an Asaro-Tiller-Grinfeld[29] istability is ruled out because the uniaxial stress is feeble. The corrugations are damped at the base of the 3D island because of the stabilizing role of the interfacial energy of the wetting layer.

The strain-induced modulation is thermally activated, and an energy barrier has to be overcome. So the development of the layer undulations requires a nucleation center, effectively decreasing the barrier energy. The step sites could act as such nucleation sites, leading to the development of corrugated layers, in agreement with some theories and experimental observations.[30,31] In Ref. 30, TEM images of corrugated layers of SiGe alloy grown on Si(001) are reported. Reference 30 describes theoretically an interesting relaxation mechanism in strained layers via surface roughening. In Ref. 32, TEM pictures of a corrugated SiGe alloy deposited on Si(001) are also reported, and the growth instability leading to modulation is credited to atomic step interactions, which is also the assumption favored in this paper. Reference 31 reports the striking result that the surface roughness has its origin in the strain-induced lowering of surface step free energies; the system under investigation is a GeSi alloy grown on top of buffer layers on a Si(100) or Ge(100) substrate.

VI. CONCLUSION

The usual kinetic Monte Carlo method is adapted to investigate off-lattice problems. In this model, the Schwoebel effect comes out as a result of the particular choice of the interaction potentiel between atoms, and the Schwoebel effect is ''felt'' by each atom located near a descending step. This model is particularly suited to the simulation of 3D islands (2D-3D growth mode and 3D growth mode). The stress field of a coherent 3D island, laying on two wetting layers, is investigated by molecular-dynamics methods. As expected, the edges of the 3D island are relaxed, but some sites, inside the 3D island, also show strong stress relaxation.

A closer look at these particular sites, located near the edges and just beneath the step site of the upper layer, discloses some strong corrugations, generated there and running through the layers at a later stage. These particular sites could act as nucleation centers, promoting the development of a corrugated layer, in agreement with some theories and experimental evidences. A lattice model could not reproduce these corrugations, which proves the usefulness of the off-lattice model developed here.

ACKNOWLEDGMENT

This work was supported by the Department of Energy under Grant No. DE-FG02-97ER2543.

[1] I. N. Stranski and Von. L. Krastanow, Akad. Wiss. Lit. Mainz Abh. Math. Naturwiss. Kl. **146**, 797 (1939); E. Bauer, H. Poppa, and G. Todd, Thin Solid Films **28**, 19 (1975).

[2] D. J. Eaglesham and M. Cerullo, Phys. Rev. Lett. **64**, 1943 (1990).

[3] D. Leonard, M. Krishnamurthy, C. M. Reaves, S. P. DenBaars, and P. M. Petroff, Appl. Phys. Lett. **63**, 3263 (1993); J. M. Moison, F. Houzay, F. Barthe, L. Leprince, E. Andre, and O. Vatel, *ibid.* **64**, 196 (1994); A. Ponchet, A. Le Corre, H. L'Haridon, B. Lambert, and S. Salaun, *ibid.* **67**, 1850 (1995).

[4] M. Volmer and A. Weber, Z. Phys. Chem. (Leipzig) **119**, 277 (1926); J. J. Metois, J. C. Heraud, and R. Kern, Surf. Sci. **78**, 191 (1978).

[5] J. A. Venables, G. D. T. Spiller, and M. Handbuecken, Rep. Prog. Phys. **47**, 399 (1984); S. Stoyanov and D. Kashiev, in *Current Topics in Material Science*, edited by E. Kaldis (North-Holland, Amsterdam, 1981).

[6] P. Jensen, H. Larralde, M. Meunier, and A. Pimpinelli, Surf. Sci. **412/413**, 458 (1998).

[7] H. T. Dobbs, D. D. Vvedensky, A. Zangwill, J. Johansson, N. Carlsson, and W. Seifert, Phys. Rev. Lett. **79**, 897 (1997).

[8] R. L. Schwoebel and E. J. Shipsey, J. Appl. Phys. **37**, 3682 (1966); R. L. Schwoebel, *ibid.* **40**, 614 (1969).

[9] P. Smilauer, M. R. Wilby, and D. D. Vvedensky, Phys. Rev. B **47**, 4119 (1993).

[10] C. Ratsch and A. Zangwill, Phys. Rev. B **50**, 14 489 (1994); C. Ratsch, M. D. Nelson, and A. Zangwill, Appl. Phys. Lett. **63**, 2348 (1993).

[11] S. Tan, A. Ghazali, and J. C. S. Levy, Surf. Sci. **369**, 360 (1996).

[12] S. Tan, A. Ghazali, and J. C. S. Levy, Surf. Sci. **392**, 163 (1997).

[13] H. Spjut and D. A. Faux, Surf. Sci. **306**, 233 (1994); W. K. Rilling, C. M. Gilmore, T. D. Andreadis, and J. A. Sprague, Can. J. Phys. **68**, 1035 (1990).

[14] C. Nagl, E. Platzgummer, M. Schmid, and P. Varga, Phys. Rev. Lett. **75**, 2976 (1995).

[15] D. Leonard, K. Pond, and P. M. Petroff, Phys. Rev. B **50**, 11 687 (1994); R. Leon, C. Lobo, J. Zou, T. Romeo, and D. J. H. Cockayne, Phys. Rev. Lett. **81**, 2486 (1998).

[16] Y. Ebiko, S. Muto, D. Suzuki, S. Itoh, K. Shiramine, T. Haga, Y. Nakata, and N. Yokoyama, Phys. Rev. Lett. **80**, 2650 (1998).

[17] M. C. Bartelt and J. W. Evans, Surf. Sci. **298**, 421 (1993); G. S. Bales and D. C. Chrzan, Phys. Rev. B **50**, 6057 (1994).

[18] F. C. Frank and J. H. van der Merwe, Proc. R. Soc. London, Ser. A **198**, 205 (1949).

[19] R. Kunkel, B. Poelsema, L. K. Verheij, and G. Comsa, Phys. Rev. Lett. **65**, 733 (1990).

[20] H. Neave, B. A. Joyce, P. J. Dobson, and N. Norton, Appl. Phys. A: Solids Surf. **31**, 1 (1983).

[21] D. D. Vvedensky and S. Clarke, Surf. Sci. **225**, 373 (1990).

[22] H. J. W. Zandvliet, H. B. Elswijk, D. Dikamp, E. J. van Loenen, and J. Dielemern, J. Appl. Phys. **70**, 2614 (1991).

[23] W. G. Hoover, Phys. Rev. A **31**, 1695 (1985).

[24] S. Christiansen, M. Albrecht, H. P. Strunk, and H. J. Maier, Appl. Phys. Lett. **64**, 3617 (1994); S. Christiansen, M. Albrecht, H. P. Strunk, P. O. Hansson, and E. Bauer, Appl. Phys. Lett. **66**, 574 (1995); T. Benabbas, P. Francois, Y. Androussi, and A. Lefebvre, J. Appl. Phys. **80**, 2763 (1996).

[25] D. A. Faux, J. R. Downes, and E. P. O'Reilly, J. Appl. Phys. **80**, 2515 (1996); L. J. Gray, M. F. Chisholm, and T. Kaplan, Appl. Phys. Lett. **66**, 1924 (1995); S. C. Jain, A. H. Harker, A. Atkinson, and K. Pinardi, J. Appl. Phys. **78**, 1630 (1995).

[26] N. Moll, M. Scheffer, and E. Pehlke, Phys. Rev. B **58**, 4566 (1998).

[27] Y. Chen and J. Washburn, Phys. Rev. Lett. **77**, 4046 (1996).

[28] W. Yu and A. Madhukar, Phys. Rev. Lett. **79**, 905 (1997).

[29] R. J. Asano and W. A. Tiller, Metall. Trans. **3**, 1789 (1972); M. A. Grinfeld, J. Nonlinear Sci. **3**, 35 (1983).

[30] J. Tersoff and F. K. Legoues, Phys. Rev. Lett. **72**, 3570 (1994).

[31] Y. H. Xie, G. H. Gilmer, C. Roland, P. J. Silverman, S. K. Buratto, J. Y. Cheng, E. A. Fitzgerald, A. R. Kortan, S. Schuppler, M. A. Marcus, and P. H. Citrin, Phys. Rev. Lett. **73**, 3006 (1994).

[32] I. Berbezier, B. Gallas, A. Ronda, and J. Derrien, Surf. Sci. **412/413**, 415 (1998).